Plasmon-Enhanced Photocurrent of Photosynthetic Pigment Proteins on Nanoporous Silver

*Vincent M. Friebe, Juan D. Delgado, David J. K. Swainsbury, J. Michael Gruber, Alina Chanaewa, Rienk van Grondelle, Elizabeth von Hauff, Diego Millo, Michael R. Jones, and Raoul N. Frese**

In a quest to fabricate novel solar energy materials, the high quantum efficiency and long charge separated states of photosynthetic pigment-proteins are being exploited through their direct incorporation in bioelectronic devices. In this work, a biohybrid photocathode comprised of bacterial reaction center-light harvesting 1 (RC-LH1) complexes self-assembled on a nanostructured silver substrate yields a peak photocurrent of 166 μA cm^{-2} under 1 sun illumination, and a maximum of 416 μA cm^{-2} under 4 suns, the highest reported to date on a bare metal electrode. A 2.5-fold plasmonic enhancement of light absorption per RC-LH1 complex is observed on the rough silver substrate. This plasmonic interaction is assessed using confocal fluorescence microscopy, revealing an increase of fluorescence yield, and radiative rate of the RC-LH1 complexes, signatures of plasmon-enhanced fluorescence. Nanostructuring of the silver substrate also enhanced the stability of the protein under continuous illumination by almost an order of magnitude relative to a nonstructured bulk silver control. Due to its ease of construction, increased protein loading capacity, stability, and more efficient use of light, this hybrid material is an excellent candidate for further development of plasmon-enhanced biosensors and biophotovoltaic devices.

1. Introduction

Through billions of years of evolution, nature has refined photosynthetic pigment-protein complexes to make highly effective use of the most abundant source of energy on our planet, solar radiation. One of these remarkable sunlight conversion systems, the reaction-center light harvesting-1 complex (RC-LH1) from the purple photosynthetic bacterium *Rhodobacter* (*R.*) *sphaeroides* (**Figure 1**a), is capable of ultrafast (<50 ps) capture and excitation energy transfer, followed by charge separation within the RC (Figure 1b,c) with near unity quantum efficiency.[1,2] This nanoscale photon-conversion unit is assembled in high yield from non-toxic, cheap, earth-abundant materials by *R. sphaeroides*. Growth capabilities under nonphotosynthetic conditions has enabled bioengineering of desirable properties including absorption profiles and redox properties of the photosynthetic protein complexes, without compromising the viability of the organism.[3,4] As a result, this tractable complex is an excellent candidate for exploitation in bioelectronics, biosensors, and biophotovoltaics.[5]

Opportunities for further enhancement of the optical properties of these biological components is enabled via hybridization with man-made materials, invoking potentially desirable phenomena that are not exhibited by the individual components, such as enhanced light-harvesting via plasmonic effects.[8,9] In the related field of thin film photovoltaics, much consideration has been given to the efficient management of incoming sunlight to compensate for the relatively low absorbance of the thin layer of photoactive component using plasmonic metal nanostructures.[10,11] Enhanced light-harvesting has been achieved by various strategies such as light scattering, coupling light with surface plasmon polaritons that propagate in the plane of the metal and the absorptive material, and localized surface plasmon resonances which create strong near-electric field enhancements.[10,11]

Although interactions between plasmonic metal nanostructures and fluorophores have been well characterized,[12] hybrid nanostructures in which photosynthetic pigment-protein complexes are interfaced with metallic nanoparticles have only recently emerged.[13,14] A predominant focus of study of these photoprotein-metal nanostructures has been on the enhancement of fluorescence which occurs as a result of the hybridization.[13] This increased emission, also known as metal-enhanced fluorescence,[15] can be significant (e.g., >500 fold),

V. M. Friebe, J. D. Delgado, J. M. Gruber,
Dr. A. Chanaewa, Prof. R. van Grondelle,
Dr. E. von Hauff, Dr. D. Millo, Dr. R. N. Frese
Department of Physics and Astronomy
LaserLaB Amsterdam
VU University Amsterdam
De Boelelaan 1081, 1081 HV Amsterdam, The Netherlands
E-mail: r.n.frese@vu.nl
Dr. D. J. K. Swainsbury, Dr. M. R. Jones
School of Biochemistry
Medical Sciences Building
University of Bristol
University Walk
Bristol BS8 1TD, UK

DOI: 10.1002/adfm.201504020

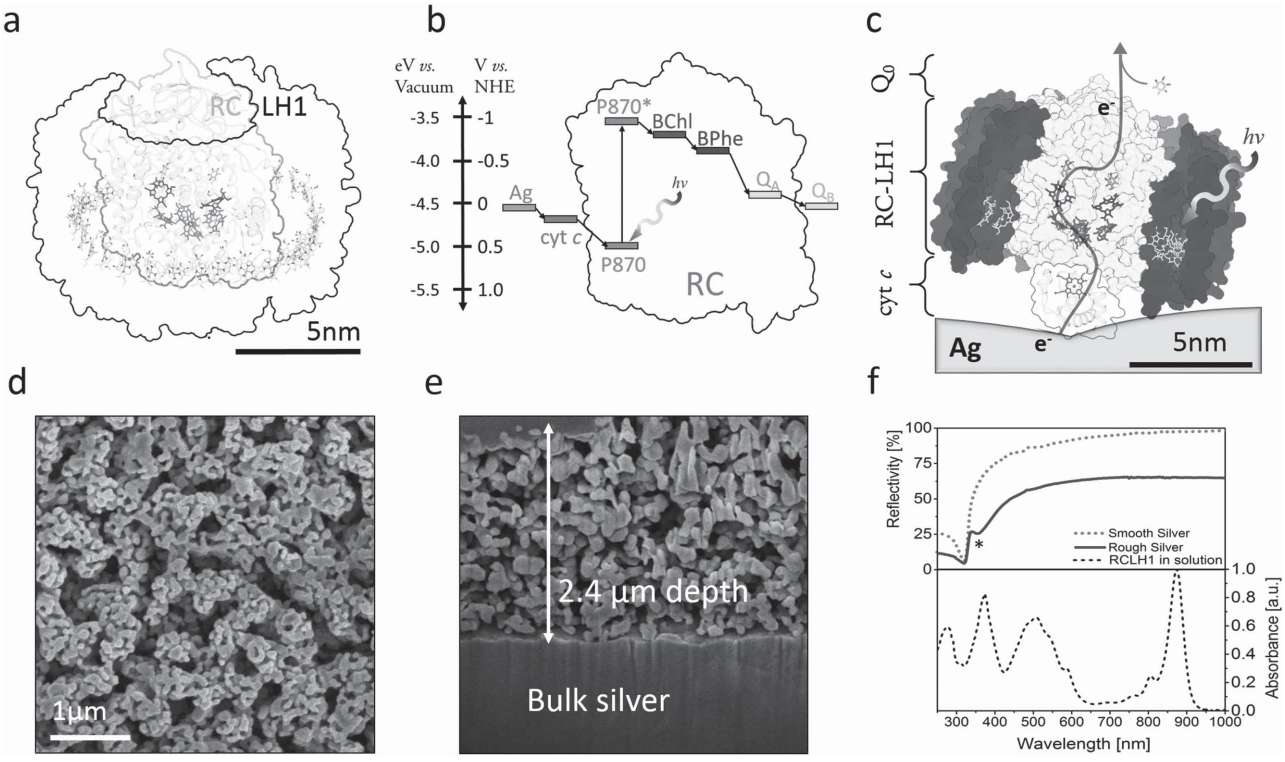

Figure 1. a) 3D rendering of an RC-LH1 pigment-protein. b) Energy diagram of electron transfer mechanism. c) Schematic of an RC-LH1 complex wired to a RS surface by cyt *c*. d) SEM of a RS surface (top view). e) SEM of a cross-sectioned RS electrode. f) SS and RS reflectivity (top) and RC-LH1 solution absorbance (bottom); * denotes the peak plasmon absorption band of the RS substrate. Panels (a,c) were generated using the crystal structure of the RC-LH1-PufX complex[6] (PDB ID: 4V9G) and USCF Chimera developed by the Resource for Biocomputing, Visualization, and Informatics at the University of California, San Francisco (supported by NIGMS P41-GM103311).[7]

and is a result of the combination of increases in extinction, radiative decay rates.[8,16] Another emergent property of these systems is the improved photostability of the fluorophores as a result of a decreased time spent in the excited state.[17] While these phenomena are interesting for the study of fundamental processes in photosynthesis, super-radiant fluorescence is not conducive to forming charge separations necessary for photocurrent generation, and thus a more suitable design is desired in bioelectronic devices. Accordingly, we have pursued novel arrangements whereby the plasmonic interactions support the rate of charge separation, yet inhibit strong radiative and non-radiative decay.

In previous work we have shown that RC-LH1 complexes and RCs can be interfaced directly with unfunctionalised smooth gold electrodes for the generation of photocurrents.[18–20] Inherent limitations in these systems for achieving high photocurrent magnitudes include low protein loading and light absorption. To address these issues, we have interfaced the RC-LH1 complexes with rough silver (RS), a large surface area material used for surface enhanced Raman spectroscopy (SERS)[21,22] and in emerging plasmon-enhanced solar cell technologies.[10,23] To delineate substrate morphology effects, the evaluation of photocurrents, fluorescence intensity, lifetime, and stability of RC-LH1 complexes on rough silver (RS|RC-LH1) were compared with those from an equivalent mechanically polished smooth silver (SS) electrode (SS|RC-LH1).

2. Results and Discussion

A rough silver surface was constructed using an electrochemical procedure[21,22] and its morphology was characterized with a scanning electron microscope (Figure 1d,e). This revealed a 2.4 μm deep, coral-like structure comprised of interconnected particles ranging from 50 to 200 nm in diameter, (Figure 1d,e), consistent with previous models that estimated an average particle diameter of 100 ± 6 nm and surface area enhancement of 20-fold.[21,22] In contrast, the SS substrate displayed a largely planar surface interspersed with ridges and grooves left over from the mechanical polishing. Reflectivity measurements on both silver surfaces in air revealed a strong absorbance band at 325 nm, typical of bulk silver (Figure 1f, top). An additional plasmon absorbance band at 375 nm (Figure 1f, asterisk) was observed on RS that approximately coincided with the Soret band of the RC-LH1 bacteriochlorins at 370 nm, and extended across the entire spectrum into the IR, as expected for a substrate containing heterogeneous nanoparticle size.[11,24–26] To exclude absorption by surface impurities during electrode preparation, the purity of rough silver was characterized by energy dispersive X-ray (EDX) analysis (Supporting Information, Figure S1). The absorbance spectrum of the RC-LH1 complex (Figure 1f) is comprised of multiple bands between 300 and 1000 nm arising from the bacteriochlorin cofactors and a broad band between 430 and 560 nm due to the absorbance of the carotenoids. This complex typically contains

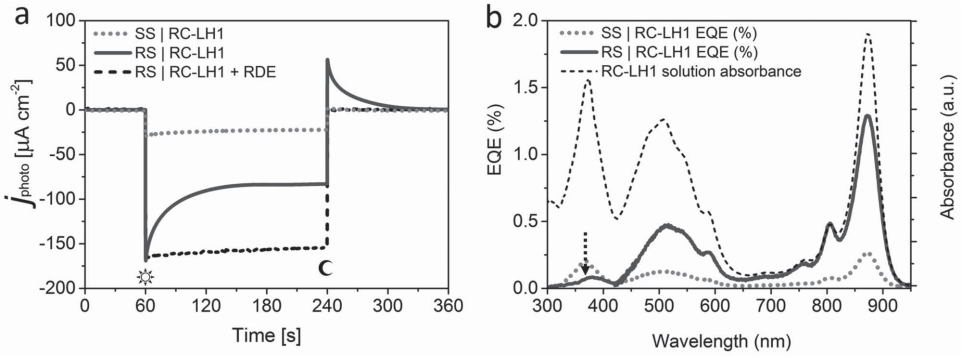

Figure 2. a) Photocurrent density produced by SS|RC-LH1 electrode (dotted) and RS|RC-LH1 (solid) electrode. The dashed line is an identical RS|RC-LH1 rotating disk electrode (RDE) operating at 500 rpm. Sun indicates light on, moon indicates light off. b) Wavelength dependent external quantum efficiency of SS|RC-LH1 and RS|RC-LH1 electrodes (left axis), RC-LH1 absorbance spectrum (right axis). Latter is normalized to the RS|RC-LH1 trace at 800 nm for comparison. *Black dotted arrow indicates parasitic absorption by the RS nanostructure.

34 bacteriochlorophylls and 15 carotenoids encapsulated in a disc shaped protein scaffold approximately 12 nm in diameter and 6 nm high (Figure 1a).[6]

Biohybrid nanostructures were constructed by sequentially drop-casting RC-LH1 complexes and the electron transfer mediator cytochrome *c* (cyt *c*) onto the prepared SS and RS surfaces (Supporting Information, Figure S2). These coated surfaces were then used as the working electrode in a three-electrode configuration liquid cell with water-soluble ubiquinone (Q_0) in the buffer solution as an electron acceptor. Illumination was provided by a tungsten-halogen lamp and a 3 cm water filter with an incident intensity of 100 mW cm^{-2}, approximating to 1 sun (Supporting Information, Figure S3). Electron transfer proceeds stepwise from the silver substrate to the cytochrome *c*, the special pair of the reaction center (P870), through the A branch and finally is captured in a quinol that diffuses out of the protein into the solution (Figure 1b).[27] Support for the proposed mechanism of electron transfer is given in Supporting Information, Figures S4 and S5.

The SS|RC-LH1 electrode yielded photocurrent densities with an average value of 27 μA cm^{-2} (**Figure 2**a) that corresponded to an external quantum efficiency (EQE = incident photons/charge carriers) of 0.022% and an apparent internal quantum efficiency (IQE_{app} = absorbed photons/charge carriers) of 16% (**Table 1**). The RC-LH1 loading ($\Gamma_{RC\text{-}LH1}$) was approximately 2.4-fold more on RS and produced an average peak cathodic photocurrent of 166 μA cm^{-2}, decaying over the next 90 s to a steady-state level of 80 μA cm^{-2} (Figure 2a). Given a RC-LH1 loading on RS of 12.1 pmol cm^{-2} this peak photocurrent corresponded to an apparent electron transfer rate (k_{app}) of 142 e$^-$ s^{-1} RC-LH1^{-1} (Table 1). Under high irradiance that saturated photocurrent, an average k_{app} of 350 e$^-$ s^{-1} RC-LH1^{-1} was achieved, which is roughly half that of an independent estimate of the maximum flux through an RC-LH1 complex of 570 e$^-$ s^{-1}.[28] This discrepancy may arise from the fact that not all of the RC-LH1 complexes are functionally interfaced with the surface, thus lowering the k_{app}. Correcting for a measured 2.4-fold greater loading, RC-LH1 complexes generated a 2.5-fold larger peak current on RS compared with SS (Table 1), likely due to plasmon-enhanced light-harvesting.

Upon cessation of 3 min of illumination, a transient anodic current was recorded for RS|RC-LH1 electrodes with a magnitude and decay lifetime that approximately corresponded to the spike of cathodic current observed during the first 90 s of illumination (Figure 2a). Current signatures of this type have been attributed to diffusion-limited transfer of charge between the working and counter electrodes, producing potential differences that dissipate in the initial dark period.[29,30] To characterize this transient photocurrent further, measurements were made with a rotating RS|RC-LH1 electrode to establish a forced convection of oxidized and reduced quinone mediator through the bulk solution. At a rotation speed of 500 rpm there was a dramatic increase in the level of the stable photocurrent up to values that were almost identical to the initial peak transient current, and the dark anodic current was lost (Figure 2a, dashed). This demonstrated that the steady state photocurrent was indeed limited by mass transport of the analyte.[29]

In measurements with monochromatic excitation, the wavelength-dependence of the calculated value for EQE showed excellent alignment with the solution absorbance spectrum of the RC-LH1 complex (Figure 2b) with no spectral shifts in

Table 1. Photocurrent density of the smooth and rough silver constructs under 100 mW cm^{-2} irradiation at –50 mV versus Ag/AgCl.

	j_{photo} [μA cm^{-2}]	$\Gamma_{RC\text{-}LH1}$ [pmol cm^{-2}]	Apparent ET rate [e$^-$s^{-1} RC-LH1^{-1}]	EQE [%]	Apparent IQE [a] [%]
Smooth silver	27 ± 5 [b]	5.0 ± 0.7	57 ± 14	0.022 ± 0.004	16 ± 2
Rough silver	166 ± 13	12.1 ± 0.9	142 ± 12	0.13 ± 0.004	39 ± 3
Enhancement factor (rough/smooth)	6.1 ± 1.2	2.4 ± 0.4	2.5 ± 0.6	6.1 ± 1.6	2.5 ± 0.4

[a]Does not take into account enhanced excitation via reflection or scattering; [b]Errors represent one standard deviation of uncertainty.

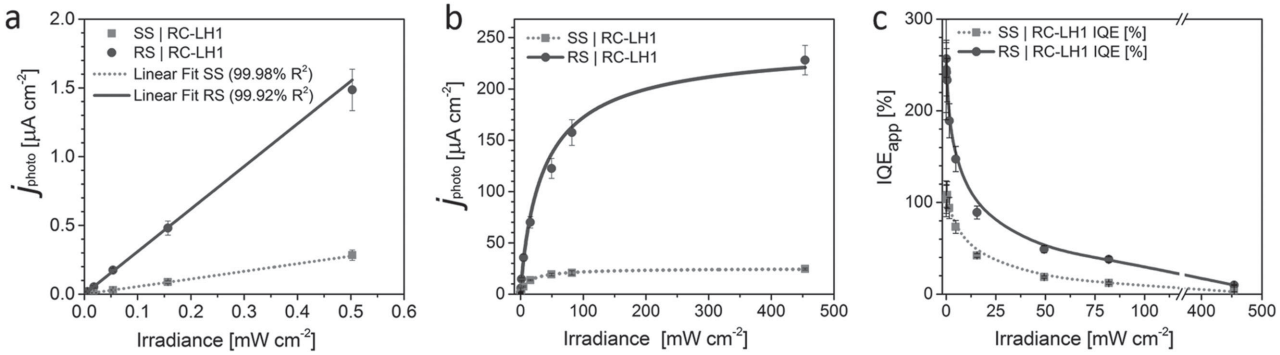

Figure 3. a) Linear increase of photocurrent density at low irradiances (<0.5 mW cm^{-2}) with linear fits. b) Photocurrent density at high irradiance. c) IQE_{app} over full irradiance range (does not assume any contribution from reflection or scattering).

the EQE spectrum on either substrate. This established that the RC-LH1 complex was the source of the photocurrent and that it had maintained its functional integrity despite the lack of a self-assembled monolayer (SAM) that is generally thought necessary to maintain protein integrity on bare metals.[31–33] The peak EQE of 1.3% at 875 nm (5 μW cm^{-2} irradiation) for the RS|RCLH1 electrode (Figure 2b) was ≈6-fold greater than the largest reported to date of 0.21% under 6 mW cm^{-2} irradiation at 875 nm using a gold surface.[34] The decreased EQE at approximately 375 nm on RS (Figure 2b, arrow) was likely due to parasitic absorption by the peak RS plasmon absorption (Figure 1f, asterisk). We suggest disparate positioning of the primary metal plasmon band (400 nm) and the primary absorptive layer absorbance (870 nm) is conducive to achieving a higher net number of charge separations because it circumvents parasitic absorption in otherwise critical light absorption regions (see Supporting Information, Figure S3 for overlap of light source and RC-LH1).

Measurement of the peak photocurrent as a function of excitation intensity revealed a linear increase below 0.5 mW cm^{-2} (**Figure 3**a). At higher irradiances, it was possible to approximately saturate the photocurrent density for both types of electrode (Figure 3b), indicating a regime where current is not limited by excitation but rather by electron flow through the system, the slowest steps of which are expected to be the diffusional limitations of the analyte. The linear region of the irradiance curve was analyzed to estimate the excitation enhancement on RS (Figure 3a). Dividing the slope of the RS electrode response by that of the SS electrode and correcting for the loading produced a value of 2.33 ± 0.5, which corresponds to the apparent amount of additional photons that the RC-LH1 complexes harvest on rough silver, assuming linear scaling.

A further approximation of the plasmonic light-harvesting enhancement was revealed by calculating the apparent internal quantum efficiency (IQE_{app}) over various irradiance intensites (Figure 3c). This clearly showed that the system is indeed more efficient at low light regimes, approaching peak values of IQE of 108 ± 15% and 256 ± 20% on SS and RS, respectively. An IQE_{app} over 100% is only possible if the optical path length of light throughout the absorptive layer has increased, or if the absorption cross-section of the pigment-protein has increased due to resonant plasmon enhancement. Accordingly, the ≈100% IQE_{app} on SS is overestimated due to reflection since ≈99% of the photons are reflected directly back through the absorptive layer. This doubles the effective photon flux throughout the absorptive layer, reducing the real IQE of the RC-LH1 complexes on SS to ≈50%. Since the intrinsic quantum efficiency of charge separation is 100%, this IQE_{app} of half that value suggests that approximately half the complexes are functionally interfaced with the smooth silver electrode. The peak IQE_{app} of 256 ± 20% on RS is the strongest indication of plasmon enhancement (Figure 3c), as it again discloses a 2.5-fold enhancement of light-harvesting per RC-LH1 with the conservative assumption that all complexes are functionally interfaced.

A large number of studies have looked at photocurrent generation by monolayers of purple bacterial reaction centers (devoid of the light-harvesting 1 ring) principally from *R. sphaeroides*, with current densities in the nA or low μA range being obtained under a wide variety of conditions (for reviews see Lu et al, Yehezkeli et al., and most recently Tan et al.).[35–37] Many studies have employed functionalization of the electrode material with a SAM for the purposes of binding and control of orientation, but it has been shown that the highest currents can be obtained by directly interfacing RCs with bare metal gold electrodes.[18,36] One exceptionally high photocurrent of 120 μA cm^{-2} on a SAM-covered gold electrode has been reported, albeit with an extremely high laser irradiance of 10 W cm^{-2} at 808 nm, revealing a significant limiting factor in these single layer systems is the capture of photons, and valorises the transition toward RC-LH1 based biophotovoltaics.[38]

In contrast, a smaller number of studies have focused on photocurrent generation by RC-LH1 complexes, beginning with reports up to 15 nA cm^{-2} on SAM functionalized gold or ITO electrodes.[39] Drop-casting *Rhodopseudomonas acidophila* RC-LH1 complexes onto unfunctionalised gold electrodes has resulted in up to 10 μA cm^{-2}, [18] and increased to 45 μA cm^{-2} by controlled deposition of a Langmuir–Blodgett film, (both studies employing ≈20 mW cm^{-2} NIR excitation).[20] In work most comparable to the present study, a peak value of 7 μA cm^{-2} with 80 mW cm^{-2} white light excitation of *R. sphaeroides* RC-LH1 complexes drop-casted onto an unfunctionalized gold electrode was reported.[34] Our average photocurrent of 166 μA cm^{-2} under 1 sun represents an approximate 20-fold increase, and our highest photocurrent recorded for a freshly prepared RS|RC-LH1 electrode under 4-suns was 416 μA cm^{-2}. To our knowledge this is far in excess of any reported photocurrent produced

by purple bacterial photosynthetic proteins on a bare metal electrode at comparable excitation intensities, and exceeded the highest photocurrent previously measured in published studies by a factor of nine.[20,36]

To investigate the source of the photocurrent enhancement obtained with RC-LH1 complexes on RS, the effects of both substrates on the fluorescence properties of RC-LH1 complexes were investigated by confocal microscopy. SS|RC-LH1 electrodes revealed a nonhomogenous fluorescence map (**Figure 4**b) that showed patterns of high-fluorescence regions that were strikingly similar to the patterns of polishing striations observed by SEM (Figure 4a). These high fluorescence regions are attributed to RC-LH1 complexes sitting on "hot spots" comprising plasmonic nanostructures inadvertently generated by the polishing procedure that are resonant with the incoming excitation and the RC-LH1 fluorophores.[40] Investigation of these hot spots revealed >100-fold enhanced fluorescence relative to more uniform surface areas, shortened fluorescence lifetimes (<20 ps), blinking events, and blue-shifted and narrowed fluorescence spectra (Supporting Information, Figure S6), all of which are signatures of strong near-field plasmon-enhanced fluorescence.[8,16] The average fluorescence lifetime outside the hotspot regions was approximately 162 ps, slightly less than the value of 206 ps for RC-LH1 complexes adsorbed on a control glass|poly-L-lysine (PLL) surface, likely due to enhanced nonradiative decay. Mean fluorescence intensity was also decreased twofold per RC-LH1 complex on SS relative to PLL (Figure 4 e), as expected for fluorophores in close proximity with a silver film.[41] Because of their infrequency, the hotspots did not strongly skew average fluorescence lifetimes and average peak fluorescence intensities for the SS surfaces.

The coated RS electrode displayed a much more intense and homogenous fluorescence topography (Figure 4d), with an average fluorescence enhancement of approximately 23-fold relative to the SS electrode under identical irradiance (Figure 4e), which corresponds to a 10-fold increase per RC-LH1 complex. In contrast to the SS electrode, fully homogenous fluorescence spectra were obtained that were identical to those obtained from RC-LH1 complexes on a PLL surface (Supporting Information, Figure S6). Fluorescence measurements revealed a significantly shortened average lifetime (77 ps) relative to RC-LH1 complexes in on the PLL surface (206 ps) and on SS electrodes (162 ps). Taken together, the decreased average fluorescence lifetime and increased average fluorescence intensity are analogous to those reported by Wientjes et al.[13] However, our observations were clearly not as strong as those observed in response to local surface plasmon resonance (LSPR) associated with isolated nanoparticles, which revealed lifetime shortening up to 20-fold and fluorescence enhancement up to 500-fold.[13] In contrast to LSPR on discrete and isolated nanoparticles, LSPRs on a semicontinuous substrate may dissociate into delocalized modes and propagate along the surface, forming surface plasmon polaritons (SPPs).[24] We suggest our observations of shortened lifetimes and enhanced fluorescence to be primarily due to interaction with such SPPs, previously characterized on similar rough silver surfaces.[26] It is well known that the magnitude of the electric field enhancement around SPPs is generally less intense than that of LSPR, which agrees well with

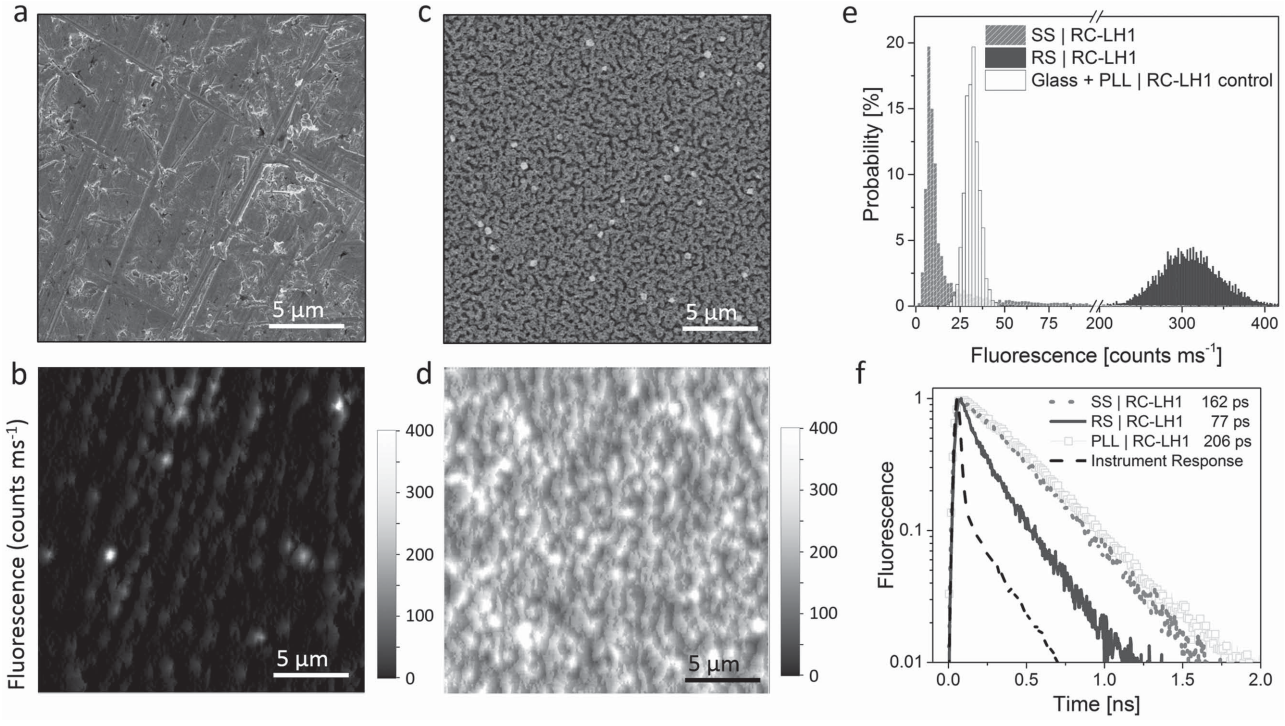

Figure 4. a) SEM image of a SS surface. b) Confocal fluorescence image of SS|RC-LH1 surface. c) SEM image of a nanostructured RS surface. d) Confocal fluorescence image of RS|RC-LH1 surface ((a–d) have identical dimensions). e) Histogram of fluorescence counts from RC-LH1 complexes on SS , RS, and on a glass/PLL surface. f) Time-correlated single-photon counting fluorescence intensity profiles for RC-LH1 complexes on SS (dotted), RS (solid), and on a glass/PLL surface (squares). The fitted lifetimes are indicated in the legend. Binning time was 4 ps and excitation was at 800 nm.

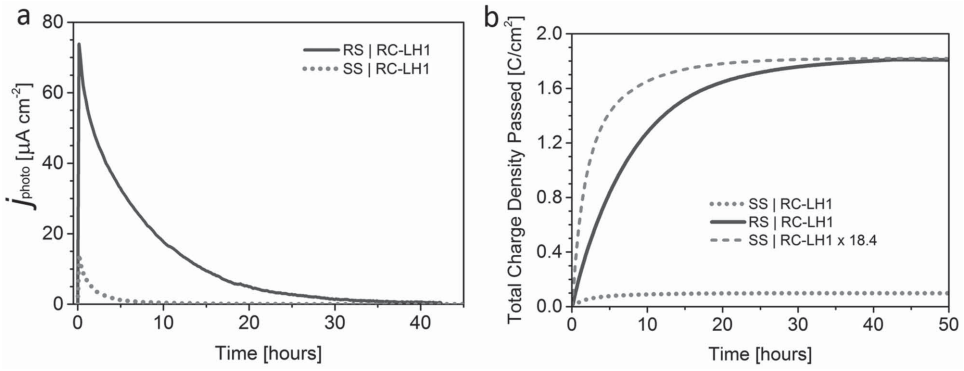

Figure 5. a) Photocurrent stability. b) Total charge density passed through the electrode.

our observations of fluorescence on RS.[11,40,42] Although the primary RS plasmon absorption band is at 375 nm (Figure 1f), the resonance extends over a wide range of wavelengths into the infrared, including the primary RC-LH1 absorption band at 870 nm, as expected for an ensemble of nanoparticles of different shapes and sizes.[11] We expect scattering also contributes to enhancing the RC-LH1 light absorption, as the larger diameter (>50 nm) nanoparticles will primarily scatter light rather than absorbing it, extending the path length of light through the absorptive layer.[11] Overall, we expect the enhanced excitation in our system to derive from a variety of mechanisms including scattering, enhanced near-field, and possibly plasmon-induced resonant energy transfer (PIRET).[43]

Although enhanced radiative and nonradiative decay are not obvious assets in a biohybrid photovoltaic device, reducing the dwell time in the excited state could lessen the formation of damaging products such as singlet oxygen and thereby increase the stability of pigment-proteins.[42] Accordingly, the stabilities of the biohybrid SS and RS electrodes were characterized under ambient conditions with near-continuous illumination (1 min dark for every 9 min illuminated) **(Figure 5)**. For both types of electrode the photocurrent gradually decreased over the time course of the measurement. Estimating the lifetime of current output from fits with two exponentials yielded a dominant component (contribution >75%) of approximately 8 h for RS|RC-LH1 electrodes as opposed to 1 h for SS counterparts, indicating an eightfold enhancement of photostability. In terms of performance, the SS|RC-LH1 electrode cycled 0.099 C cm^{-2} over 48 h, while the RS|RC-LH1 electrode cycled 1.8 C cm^{-2} over the same period (Figure 5b), an 18-fold increase. Accounting for loading, this corresponded to an average of 1.55×10^6 turnovers per RC-LH1 complex on RS and 0.206×10^6 on SS over the first 2 d, an eightfold stability enhancement per complex, corresponding well with the lifetime analysis. We speculate that the origin of this increased photostability is due to the decreased dwell time in the excited state resulting from the enhanced radiative rate decay of RC-LH1 on RS. Overall, we report stability on the order of days in ambient conditions, with turnover rates and lifetimes comparable to RC-LH1 complexes in vivo.

3. Conclusion

This work demonstrates that significant enhancements of photocurrent generation and stability can be achieved by simple and direct interfacing of photosynthetic proteins with a plasmonic metal surface. This was achieved by a simple method of drop casting photosynthetic protein-complexes onto an electrochemically roughened silver electrode without the use of a SAM, resulting in a peak photocurrent of 416 μA cm^{-2}, exceeding previously reported comparable studies by a factor of nine.[20,36] Confocal microscopy revealed an increased fluorescence yield and faster RC-LH1 radiative rates, indicating detrimental processes toward charge separation. Despite this, RC-LH1 complexes netted a 2.5-fold increased photocurrent due to plasmon-enhanced light-harvesting on RS compared with SS. The increased stability of the RC-LH1 complex was another promising property of the biohybrid RS electrode. Enhanced charge separation and stability of this system strongly supports further development of the fabrication procedures and cell design, particularly the exclusion of oxygen, and could lead to systems that are stable over days under continuous illumination. Finally, the increase in loading of the RC-LH1 complex on moving from a SS to RS substrate was only a modest 2.4-fold, and further enhancements could be obtained through oriented 3D electrode architectures that mimic the multilayer architectures seen in the photosynthetic membranes of the chloroplasts and photosynthetic bacteria that constitute nature's solar powerpacks.

4. Experimental Section

Materials: Horse heart cytochrome *c* (cyt *c*) and 2,3-dimethoxy-5-methyl-p-benzoquinone (Q_0) were purchased from Sigma-Aldrich. Milli-Q water (Millipore, Massachusetts) was used in all preparations and procedures.

RC-LH1 Mutant: DNA encoding RCs modified with a poly-histidine tag at the C-terminus of the M-subunit[5] was cloned as a 1841 bp XbaI-BamHI restriction fragment into plasmid pRKEH10,[3] which is a derivative of broad-host-range vector pRK415 containing a 6.2 kb EcoRI–HindIII fragment encoding pufQBALMX. The resulting plasmid was named pvBALMtX, and was introduced into *R. sphaeroides* strain DD13 by conjugative transfer as previously described.[3] The resulting transconjugant strains contained His-tagged RC-LH1 complexes but lacked LH2 antenna proteins.

RC-LH1 Purification: This protocol was adapted from that previously published for His-tagged RCs.[5] Briefly, *R. sphaeroides* DD13 expressing plasmid pvBALMtX was grown under semiaerobic dark conditions in M22 medium to a total volume of 12 L.[44] Cells were harvested by centrifugation, resuspended in 20×10^{-3} M Tris (pH 8) containing DNAse I and two complete EDTA-free Protease Inhibitor tablets (Roche) and lysed at 20 000 psi in a cell disruptor (Constant Systems).

Debris was removed by centrifugation at 26 890 RCF for 15 min at 4 °C. Membranes in the supernatant were solubilised by the addition of 200 × 10^{-3} M NaCl and 2% (w/v) n-dodecyl β-D-maltopyranoside (DDM) at room temperature in the dark for 1 h and insoluble material was separated by ultracentrifugation at 100 000 RCF for 30 min at 4 °C. The supernatant was loaded onto a 20 mL HisPrep FF Ni-NTA column (GE Healthcare) pre-equilibrated with 100 mL 20 × 10^{-3} M Tris (pH 8), containing 200 × 10^{-3} M NaCl, 20 × 10^{-3} M imidazole, and 0.04% w/v DDM (equilibration buffer). After loading, the column was washed with 400 mL equilibration buffer and RC-LH1 complexes were eluted with the same buffer supplemented with 500 × 10^{-3} M imidazole. Complexes were further purified on a Superdex 200 16/60 gel filtration column (GE Healthcare) pre-equilibrated with 200 mL of 20 × 10^{-3} M Tris (pH 8) containing 0.04% w/v DDM. Fractions containing RC-LH1 complexes were pooled and concentrated. The ratio of absorbance of bacteriochlorophyll at 875 nm to protein at 280 nm was 1.9, which corresponded to contaminating proteins being undetectable. Protein was stored in 20 × 10^{-3} M Tris (pH 8), 0.04% DDM at −80 °C.

Reflectivity: Diffuse reflectance spectroscopy was used to measure the reflectivity of the silver substrates in diffuse reflectance mode with the sample at 8° to the incoming beam placed in the back position of the integrating sphere, enabling capture of scattered light and specificity to light extinction on the substrate (Perkin Elmer Lambda 900 UV/VIS/NIR Spectrometer, PELA-1020 Integrating Sphere).

Fabrication of Silver RC-LH1 Electrodes: Planar disk polycrystalline silver working electrodes of 2 mm diameter (CHI Instruments) were mechanically polished to a mirror-like finish using Al_2O_3 lapping films of successively finer grain size from 5 to 1 μm (Thor Labs), followed by rinsing of the electrode with milli-Q water after each polishing step. Rough silver electrodes were prepared by subjecting the polished Ag electrodes to an electrochemical procedure consisting of four oxidation/reduction cycles in 0.1 M KCl, as described elsewhere.[21,22] Smooth and rough silver electrodes were drop-casted with 7.5 μL of 51.5 × 10^{-6} M RC-LH1 complexes for 15 min in the dark at 4 °C. Unbound protein was removed by controlled, repeated dipping in 20 × 10^{-3} M Tris (pH 8) at 4 °C using a home-built dipping apparatus. Subsequently, coated electrodes were incubated for 5 min in a solution containing 200 × 10^{-6} M cyt *c* in 20 × 10^{-3} M Tris (pH 8), followed by another round of rinsing to remove unbound cyt *c*.

Photochronoamperometry: Silver working electrodes (Metrohm Autolab, 3 mm diameter) drop-casted with RC-LH1 complexes and cyt *c* were placed into a photoelectrochemical cell also fitted with a Ag/AgCl/3M KCl reference electrode and a platinum counter electrode (Metrohm Autolab BV, Utrecht, the Netherlands) in a working solution of 1.5 × 10^{-3} M Q_0 in 20 × 10^{-3} M Tris (pH 8). A PGSTAT128N potentiostat (Metrohm Autolab) was used to control the three-electrode cell, a bias potential of −50 mV versus Ag/AgCl being applied for all experiments (approximating to the dark open circuit potential). The entire working electrode was homogeneously illuminated with a home-built 150 W tungsten halogen lamp (HXL 64242, Osram) at an irradiance of 100 mW cm^{-2} (approximately 1 sun) at the electrode surface. A series of neutral density filters were employed to vary the irradiance, which was measured with a thermopile detector (Coherent Powermax 2). To study diffusion-limited process in the cell, force convection of the analyte by the working electrode was achieved via an Autolab RDE rotating disc electrode (Metrohm Autolab). All photocurrent measurements were performed under ambient conditions, in air at room temperature.

Quantification of RC-LH1 Loading: Upon completion of photocurrent measurements, silver working electrodes were hermetically sealed into a 500 μL Eppendorf microcentrifuge tube containing 250 μL of a solution of 80% acetone and 20% milli-Q water saturated with Na_2CO_3, then vortexed for 30 s in the dark, followed by sonication (30 s). The electrode was removed and the absorbance spectrum of the solution recorded. The loading of RC-LH1 complexes on each electrode (Γ_{RCLH1}, (mol cm^{-2})) was estimated using an extinction coefficient at 770 nm for Bchl *a* in 80% acetone of (69.3 ± 0.3) × 10^{-3} M cm^{-1} ,[45] and by assuming each *R. sphaeroides* RC-LH1 complexes contains 32 molecules of BChl *a*.[6] Full removal of photosynthetic material was confirmed by the absence of a photocurrent on the pigment-extracted electrodes and absence of any detectable absorbance after completely grinding the electrode, fragmenting the rough silver layer.

Measurement and Calculation of EQE and IQE: The EQE is defined as the ratio of generated charge carriers to the number incident photons. To measure the wavelength dependence of EQE, the 150 W white light source was passed through a monochromator resulting in an illumination intensity of 25 μW cm^{-2} at 880 nm and a FWHM of 2 nm, measured with an Ocean Optics fiber optic spectrometer (USB2000 UV–vis) and a Coherent UV–vis Si power meter, respectively. Photocurrents were measured while the excitation wavelength was scanned at a rate of 1 nm per second from 400 to 900 nm and then from 900 to 400 nm, and the two scans were then averaged. EQE at each wavelength was calculated from the measured photocurrent density (*J*) and the incident irradiance (*I*) at that wavelength using the equation

$$\mathrm{EQE} = 100 \times \left(J \cdot \hbar\omega \right) / \left(e \cdot I \right) \quad (1)$$

where *e* is the elementary charge of an electron, $\hbar$ is Planck's constant, and ω is the frequency of light.

The IQE is the ratio of the number of generated charge carriers to the number of photons absorbed per second as previously calculated.[20,46]

Confocal Fluorescence Microscopy and Lifetime Measurements: The adsorption profile of RC-LH1 complexes on silver working electrodes was measured using a home-built confocal fluorescence microscope described elsewhere.[47,48] Excitation at 800 nm was achieved using a Ti:sapphire laser system (Coherent, Mira900) that yielded 200 fs pulses at a repetition rate of 76 MHz. The excitation was focused to a diffraction limited spot at the water–electrode interface, and fluorescence emission resolved using a dichroic beam splitter (815 dclp, Chroma Technology). The working electrode was raster scanned in a home-built holder mounted into a closed loop 2D piezo stage (P-731.8C XY PZT Flexure Stage, Physik Instrumente) controlled by a digital four-channel controller (E-710.4LC, Physik Instrumente). Fluorescence intensity and lifetime profiles were measured using a single photon avalanche diode (PD-050-CTE, Micro Photon Devices) coupled to a time-correlated single photon counting module (PicoHarp 300, Picoquant). Fluorescence spectra with 1 s integration times were obtain by dispersing the fluorescence emission with a grating (HR830/800 nm, Optometrics) onto a nitrogen-cooled back-illuminated CCD camera (Spec10:100BR, Princeton Instruments, Roper Scientific B.V.). The working buffer for all experiments consisted of 20 × 10^{-3} M Tris (pH 8). To enhance RC-LH1 photostability, anoxic conditions in the working buffer were achieved via an oxygen scavenger system described previously.[48] The confocal microscopy images in Figure 3 were taken under 200 nW excitation at 800 nm with identical exposure times per pixel (200 × 200 pixels, smoothing 3, identical fluorescence counts).

Scanning Electron Microscopy and X-Ray Photoelectron Spectroscopy: SEM images were taken with a FEI Verios high resolution SEM. Samples were prepared and immediately stored under nitrogen until imaged. Images were taken with an accelerating voltage between 1 and 5 kV under a vacuum (10^{-6} mbar). An EDX microanalysis module by Oxford provided information on the elemental composition of the surface of the electrodes. Focused-ion beam etching was performed with a FEI Helios nanolab dual beam SEM and enabled cross-sectional imaging of the RS substrate.

Supporting Information

Supporting Information is available from the Wiley Online Library or from the author.

Acknowledgements

M.R.J. and D.J.K.S. acknowledge support from the Biotechnology and Biological Sciences Research Council of the UK (Project No.

BB/I022570/1). R.N.F. acknowledges support from the Dutch science foundation NWO for a vidi grant, D.M. for a veni grant (No. 722.011.003). M.R.J., R.N.F., D.J.K.S., V.M.F., and J.D.D. acknowledge support via EU COST Action TD1102—Photosynthetic proteins for technological applications: biosensors and biochips (PHOTOTECH). AMOLF Institute (Science Park, Amsterdam) is gratefully acknowledged for providing access to FIB etching, SEM, and EDX characterization. Rinke Wijngaarden and Leo Polak are acknowledged for providing access for diffuse reflectance spectroscopic characterization. Dr. Laura M. Roy is acknowledged for assistance in manuscript preparation.

Received: September 21, 2015
Revised: October 16, 2015
Published online: December 7, 2015

[1] R. Van Grondelle, J. P. Dekker, T. Gillbro, V. Sundstrom, *Biochim. Biophys. Acta, Bioenerg.* **1994**, *1187*, 1.
[2] C. A. Wraight, R. K. Clayton, *Biochim. Biophys. Acta* **1974**, *333*, 246.
[3] M. R. Jones, G. J. Fowler, L. C. Gibson, G. G. Grief, J. D. Olsen, W. Crielaard, C. N. Hunter, *Mol. Microbiol.* **1992**, *6*, 1173.
[4] *The Purple Phototrophic Bacteria* (Eds: C. N. Hunter, F. Daldal, M. C. Thurnauer, J. T. Beatty), Advances in Photosynthesis and Respiration, Vol. *28*, Springer, Dordrecht, The Netherlands **2009**.
[5] D. J. K. Swainsbury, V. M. Friebe, R. N. Frese, M. R. Jones, *Biosens. Bioelectron.* **2014**, *58*, 172.
[6] P. Qian, M. Z. Papiz, P. J. Jackson, A. a. Brindley, I. W. Ng, J. D. Olsen, M. J. Dickman, P. a. Bullough, C. N. Hunter, *Biochemistry* **2013**, *52*, 7575.
[7] E. F. Pettersen, T. D. Goddard, C. C. Huang, G. S. Couch, D. M. Greenblatt, E. C. Meng, T. E. Ferrin, *J. Comput. Chem.* **2004**, *25*, 1605.
[8] S. Mackowski, *J. Phys. Condens. Matter* **2010**, *22*, 193102.
[9] S. Mackowski, S. Wörmke, A. J. Maier, T. H. P. Brotosudarmo, H. Harutyunyan, A. Hartschuh, A. O. Govorov, H. Scheer, C. Bräuchte, *Nano Lett.* **2008**.
[10] H. a. Atwater, A. Polman, *Nat. Mater.* **2010**, *9*, 205.
[11] S. Linic, P. Christopher, D. B. Ingram, *Nat. Mater.* **2011**, *10*, 911.
[12] Y. Fu, J. Zhang, J. R. Lakowicz, *Biochem. Biophys. Res. Commun.* **2008**, *376*, 712.
[13] E. Wientjes, J. Renger, A. G. Curto, R. Cogdell, N. F. van Hulst, *Nat. Commun.* **2014**, *5*, 4236.
[14] I. Kim, S. L. Bender, J. Hranisavljevic, L. M. Utschig, L. Huang, G. P. Wiederrecht, D. M. Tiede, *Nano Lett.* **2011**, *11*, 3091.
[15] C. D. Geddes, J. R. Lakowicz, *J. Fluoresc.* **2002***12*, 121.
[16] E. Wientjes, J. Renger, A. G. Curto, R. Cogdell, N. F. van Hulst, *Phys. Chem. Chem. Phys.* **2014**, *16*, 24739.
[17] H. Cang, Y. Liu, Y. Wang, X. Yin, X. Zhang, *Nano Lett.* **2013**, *13*, 5949.
[18] M.-J. den Hollander, J. G. Magis, P. Fuchsenberger, T. J. Aartsma, M. R. Jones, R. N. Frese, *Langmuir* **2011**, *27*, 10282.
[19] G. J. Magis, M.-J. den Hollander, W. G. Onderwaater, J. D. Olsen, C. N. Hunter, T. J. Aartsma, R. N. Frese, *Biochim. Biophys. Acta* **2010**, *1798*, 637.
[20] M. Kamran, J. D. Delgado, V. Friebe, T. J. Aartsma, R. N. Frese, *Biomacromolecules* **2014**, *15*, 2833.
[21] D. Millo, A. Ranieri, P. Gross, H. K. Ly, M. Borsari, P. Hildebrandt, G. J. L. Wuite, C. Gooijer, G. van der Zwan, *J. Phys. Chem. C* **2009**, *113*, 2861.
[22] D. D. Tuschel, J. E. Pemberton, J. E. Cook, *Langmuir* **1986**, *2*, 380.
[23] F.-J. Haug, T. Söderström, O. Cubero, V. Terrazzoni-Daudrix, C. Ballif, *J. Appl. Phys.* **2008**, *104*, 064509.
[24] N. J. Borys, E. Shafran, J. M. Lupton, *Sci. Rep.* **2013**, *3*, 2090.
[25] T. Tan, C. Tian, Z. Ren, J. Yang, Y. Chen, L. Sun, Z. Li, A. Wu, J. Yin, H. Fu, *Phys. Chem. Chem. Phys.* **2013**, *15*, 21034.
[26] S. K. Kim, H. S. Ee, W. Choi, S. H. Kwon, J. H. Kang, Y. H. Kim, H. Kwon, H. G. Park, *Appl. Phys. Lett.* **2011**, *98*, 2.
[27] M. Kamran, V. M. Friebe, J. D. Delgado, T. J. Aartsma, R. N. Frese, M. R. Jones, *Nat. Commun.* **2015**, *6*, 6530.
[28] F. Comayras, C. Jungas, J. Lavergne, *J. Biol. Chem.* **2005**, *280*, 11214.
[29] S. M. Mirvakili, J. E. Slota, A. R. Usgaocar, A. Mahmoudzadeh, D. Jun, M. N. Mirvakili, J. T. Beatty, J. D. W. Madden, *Adv. Funct. Mater.* **2014**, *24*, 4789.
[30] P. N. Ciesielski, D. E. Cliffel, G. K. Jennings, *J. Phys. Chem. A* **2011**, *115*, 3326.
[31] N. Lebedev, S. A. Trammell, A. Spano, E. Lukashev, I. Griva, J. Schnur, *J. Am. Chem. Soc.* **2006**, *128*, 12044.
[32] M. Kondo, Y. Nakamura, K. Fujii, M. Nagata, Y. Suemori, T. Dewa, K. Iida, A. T. Gardiner, R. J. Cogdell, M. Nango, *Biomacromolecules* **2007**, *8*, 2457.
[33] H. Yaghoubi, Z. Li, D. Jun, R. Saer, J. E. Slota, M. Beerbom, R. Schlaf, J. D. Madden, J. T. Beatty, A. Takshi, *J. Phys. Chem. C* **2012**, *116*, 24868.
[34] H. Yaghoubi, E. Lafalce, D. Jun, X. Jiang, J. T. Beatty, A. Takshi, *Biomacromolecules* **2015**, *16*, 1112.
[35] O. Yehezkeli, R. Tel-Vered, D. Michaeli, I. Willner, R. Nechushtai, *Photosynth. Res.* **2014**, *120*, 71.
[36] S. C. Tan, S. K. Ravi, *Energy Environ. Sci.* **2015**, *8, 2551*.
[37] Y. Lu, J. Xu, B. Liu, J. Kong, *Biosens. Bioelectron.* **2007**, *22*, 1173.
[38] R. Das, P. J. Kiley, M. Segal, J. Norville, a. A. Yu, L. Wang, S. A. Trammell, L. E. Reddick, R. Kumar, F. Stellacci, N. Lebedev, J. Schnur, B. D. Bruce, S. Zhang, M. Baldo, *Nano Lett.* **2004**, *4*, 1079.
[39] M. Kondo, K. Iida, T. Dewa, H. Tanaka, T. Ogawa, S. Nagashima, K. V. P. Nagashima, K. Shimada, H. Hashimoto, A. T. Gardiner, R. J. Cogdell, M. Nango, *Biomacromolecules* **2012**, *13*, 432.
[40] Y. Lu, G. L. Liu, J. Kim, Y. X. Mejia, L. P. Lee, *Nano Lett.* **2005**, *5*, 119.
[41] J. R. Lakowicz, Y. Shen, S. D'Auria, J. Malicka, J. Fang, Z. Gryczynski, I. Gryczynski, *Anal. Biochem.* **2002**, *301*, 261.
[42] J. Li, S. K. Cushing, P. Zheng, F. Meng, D. Chu, N. Wu, *Nat. Commun.* **2013**, *4*, 2651.
[43] J. Li, S. K. Cushing, F. Meng, T. R. Senty, A. D. Bristow, N. Wu, *Nat. Photonics* **2015**, *9*, 601.
[44] M. R. Jones, M. Heer-Dawson, T. A. Mattioli, C. N. Hunter, B. Robert, *FEBS Lett.* **1994**, *339*, 18.
[45] H. P. Permentier, K. A. Schmidt, M. Kobayashi, M. Akiyama, C. Hager-Braun, S. Neerken, M. Miller, J. Amesz, *Photosynth. Res.* **2000**, *64*, 27.
[46] P. N. Ciesielski, C. J. Faulkner, M. T. Irwin, J. M. Gregory, N. H. Tolk, D. E. Cliffel, G. K. Jennings, *Adv. Funct. Mater.* **2010**, *20*, 4048.
[47] D. Rutkauskas, V. Novoderezkhin, R. J. Cogdell, R. van Grondelle, *Biochemistry* **2004**, *43*, 4431.
[48] T. P. J. Krüger, V. I. Novoderezhkin, C. Ilioaia, R. van Grondelle, *Biophys. J.* **2010**, *98*, 3093.